

## **HYDROSTATIC PRESSURE SENSOR BASED ON A GOLD-COATED FIBER MODAL INTERFEROMETER USING LATERAL OFFSET SPLICING OF SINGLE MODE FIBER**

**D. Chen<sup>1,\*</sup> and X. Cheng<sup>2</sup>**

<sup>1</sup>Institute of Information Optics, Zhejiang Normal University, Jinhua 321004, China

<sup>2</sup>Photonics Research Centre, Department of Electrical Engineering, The Hong Kong Polytechnic University, Hung Hom, Kowloon, Hong Kong SAR, China

**Abstract**—A novel hydrostatic pressure sensor based on a gold-coated fiber modal interferometer (FMI) is proposed and demonstrated. Two single mode fibers (SMFs) are spliced with a lateral offset which forms a single-end FMI. The single-end FMI is gold-coated to enhance the reflectivity and to avoid the influence of any unwanted light from getting into the sensor. Relative reflection spectra of the proposed FMIs with different sensing SMF lengths or different lateral offsets are experimentally investigated. A high hydrostatic pressure sensor test system is proposed for the testing of the proposed FMI pressure sensor. The performance of a gold-coated FMI pressure sensor based on a 12-mm sensing SMF has been experimentally investigated. The proposed pressure sensor has a sensing range from 0 to 42 MPa and a sensitivity of 53 pm/MPa.

### **1. INTRODUCTION**

Optical fiber sensors [1–13] have attracted considerable attention in the past several decades due to their wide applications for a great variety of measurements such as temperature, strain, chemical concentration, refractive index, hydrostatic pressure and their advantages such as small size, light weight, high sensitivity, multiplexing capability, and immunity to electromagnetic interference. Among them, several hydrostatic pressure sensing techniques have been developed, which

---

*Received 23 December 2011, Accepted 23 January 2012, Scheduled 30 January 2012*

\* Corresponding author: Daru Chen (daru@zjnu.cn).

include hydrostatic pressure sensors based on birefringent fibers [14–16], photonic crystal fibers (PCFs) (or microstructured fibers) [17–24], fiber Bragg gratings (FBGs) [18], and Fabry-Pérot interferometers (FPIs) [25–27]. Hydrostatic pressure sensors based on birefringent fibers are not compact since they usually need non-fiber components to detect the pressure-induced phase or use the fiber Sagnac interferometer with a relatively long sensing fiber. PCFs [28–32] are the great success in the history of optical fibers, which have achieved excellent properties in birefringence [33–40], dispersion [41–51], single polarization single mode [52–54], nonlinearity [55], and effective mode area [56–58], and also excellent performances in the applications of fiber lasers [59–61] and nonlinear optics [62–65] over the past several years. PCFs have also further improved optical fiber sensors and have been used for strain sensing [66], gas sensing [67], biochemical sensing [68], refractive index sensing [69] and temperature sensing [70]. More recently, several hydrostatic pressure sensors based on the PCF are reported and demonstrated [17–24]. However, the demonstrated PCF pressure sensors are neither compact due to the PCF with lengths of several tens of centimeters nor low cost due to the relatively complex fabrication processing. The fiber Bragg grating (FBG) is not very sensitive to the hydrostatic pressure and the fabrication needs high cost equipments, which is the same for the FPIs. We have recently proposed a hydrostatic pressure sensor based on mode interference of a few mode fiber [71], which also needs a 37-cm sensing fiber.

In this paper, we use the inexpensive single mode fiber (SMF) to fabricate a novel fiber modal interferometer (FMI) based on lateral offset splicing, which is coated with gold for hydrostatic pressure sensing. The gold-coated SMF itself acts as the pressure sensing element and forms the FMI due to the interference of the cladding mode light and the core mode light. A high hydrostatic pressure sensor test system is conducted and a linear relationship between the hydrostatic pressure and the wavelength shift of the relative reflection spectrum of the FMI pressure sensor has been presented.

## 2. EXPERIMENTAL SETUP AND PRINCIPLE

Figure 1(a) shows the structure of the proposed FMI. The sensing SMF with a length ( $L$ ) using as the hydrostatic pressure sensing element is spliced to the guiding SMF (using as the optical guiding medium) with a lateral offset ( $h$ ). Note that the sensing SMF should be well cleaved to provide a good air-silica interface as one mirror of the FMI. The FMI is coated with gold to ensure the reflectivity of the spherical surface and also to avoid the influence of any unwanted light from getting into the

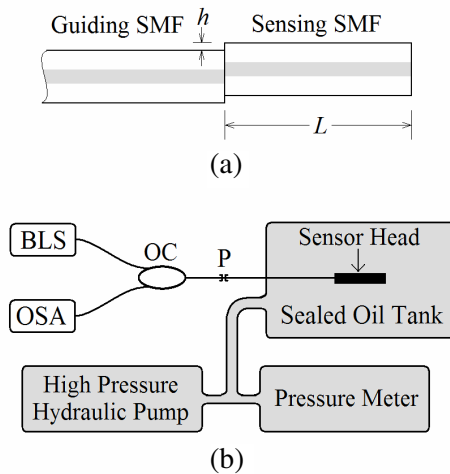


**Figure 1.** (a) Structure of the FMI sensor head. (b) Schematic diagram of a hydrostatic pressure sensing test system. BLS: broadband light source; OSA: optical spectrum analyzer; OC: optical coupler.

sensor when the sensor head is inserted into the liquid. Note that when there is no gold coating for the sensing SMF of the FMI, the light of the fiber cladding mode of the sensing SMF will be leaky to the liquid and the mode index of the fiber cladding mode is also dependent on the index of the liquid which results in crosstalk between the pressure and the index (of the liquid) for sensing application. Figure 1(b) shows the experimental setup of the hydrostatic pressure sensing test system. A broadband light source (BLS) provides output light with a broadband wavelength range from 1410 nm to 1640 nm. The broadband light is injected into the FMI pressure sensor through a broadband optical coupler (OC). The reflective light is detected by an optical spectrum analyzer (OSA), which has a resolution of 0.02 nm. There is an FC/PC connector shown as the P point in Figure 1(b) in the pressure sensing test system. The FMI pressure sensor is inserted into a sealed oil tank, where the hydrostatic pressure is controlled by a high pressure hydraulic pump and measured by an electronic pressure meter. The FMI pressure sensor should be kept straight and well fixed inside the sealed oil tank.

When the broadband light from the guiding SMF is injected into the FMI, part of the light power will be distributed in the core mode of the sensing SMF and some of the light power propagates in the cladding mode. They will be partially reflected by the end (silica-gold

interface) of the sensing SMF, which finally result in the interference in the guiding SMF. When the power back to the guiding SMF for the core mode light and the cladding mode light is  $I_1$  and  $I_2$ , respectively, the measured intensity in the guiding SMF is given by

$$I = I_1 + I_2 + 2\sqrt{I_1 I_2} \cos[4\pi \Delta n L / \lambda] \quad (1)$$

where  $L$  is the length of the sensing SMF and  $\lambda$  is the light wavelength in vacuum.  $\Delta n = n_2 - n_1$  is the difference of the mode indices of the core mode ( $n_1$ ) and the cladding mode ( $n_2$ ) of the sensing SMF. The wavelength spacing of the interfering spectrum according to Equation (1) is given by

$$\Delta \lambda \approx \frac{\lambda^2}{2\Delta n L} \quad (2)$$

When the sensing SMF is subjected to a hydrostatic pressure, the stress induced by the pressure will result in refractive index change due to the photoelastic effect. The refractive index of the pure silica subjected to the pressure is given by [18]

$$\begin{aligned} n_x &= n_0 - C_1 \sigma_x - C_2 (\sigma_y + \sigma_z) \\ n_y &= n_0 - C_1 \sigma_y - C_2 (\sigma_x + \sigma_z) \end{aligned} \quad (3)$$

where  $\sigma_x$ ,  $\sigma_y$  and  $\sigma_z$  are the stress components,  $C_1 = 6.5 \times 10^{-13} \text{ m}^2/N$  and  $C_2 = 4.2 \times 10^{-12} \text{ m}^2/N$  are the stress-optic coefficients of pure silica. Thus,  $\Delta n$ ,  $n_1$ , and  $n_2$  are dependent on the hydrostatic pressure applied on the sensing SMF. Note that there may be several cladding modes in the sensing fiber which will results in a relatively complex interference spectrum.

### 3. EXPERIMENTAL RESULTS

The red dotted curve shown in Figure 2(a) is the measured output spectrum of the BLS due to Fresnel reflection of the open FC/PC connector (labeled P in Figure 1(b)), which is used as the spectrum reference in this Letter. When the FMI based on a 12-mm sensing SMF is connected to P and suspended in air, the measured output spectrum of the FMI is shown as the black solid curve in Figure 2(a). Figure 2(b) shows the relative reflection spectra of the three FMIs based on the sensing SMFs with lengths of 44.5 mm (blue dotted curve), 21.5 mm (green dashed curve) and 12 mm (black solid curve), respectively. Note that the relative reflection spectrum is the measured output spectrum of the FMI after subtracting the output spectrum of the BLS. The wavelength spacing (around 1500 nm) of the relative reflection spectra of the three FMIs is 17 nm, 10.5 nm, and 5 nm, respectively and the

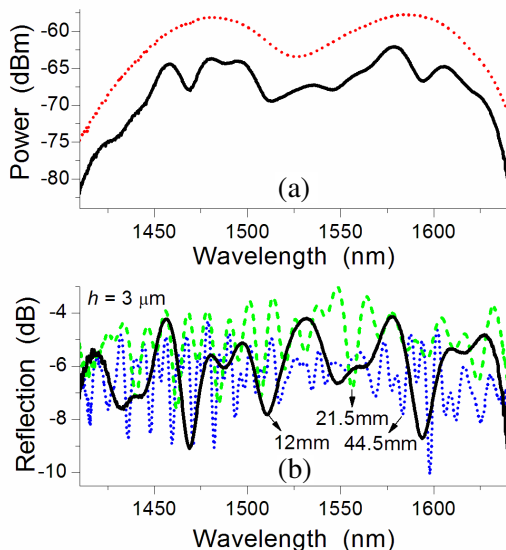


**Figure 2.** (a) Measured spectra of the BLS due to the Fresnel reflection of the FC/PC connector (red dotted curve) and the uncoated FMI (black solid curve). (b) Relative reflection spectra of the three uncoated FMIs with SMF lengths of 44.5 mm (blue dotted curve), 21.5 mm (green dashed curve) and 12 mm (black solid curve), respectively.

largest extinction ratio (ER) is about 5 dB. Since there is the possibility that more than one cladding mode is exited in the sensing SMF, multimode interference may happen in the guiding SMF which results in a relative complex relative reflection spectrum of the FMI.

The ER can be improved by employing a larger lateral offset where the guiding SFM can receive more power of the cladding mode light. As shown in Figure 3, two FMIs with a lateral offset  $h = 4.5 \mu\text{m}$  have relative reflection spectra with a larger ER than the FMI with a lateral offset  $h = 3 \mu\text{m}$ , however, which also have larger insert loss. Figure 3 shows the relative reflection spectrum of the gold-coated FMI based on a 12-mm sensing SMF with a lateral offset  $h = 3 \mu\text{m}$  (red dotted curve), where one can observe that the reflectivity of the sensing SMF end is greatly enhanced (about 15 dB). The gold coating totally covers the sensing SMF, which enhances the reflectivity of the fiber end and avoids the influence of any unwanted light from getting into the sensor.

When the gold-coated FMI is inserted to the sealed oil tank, the mode indices of the cladding mode and the core mode of the sensing

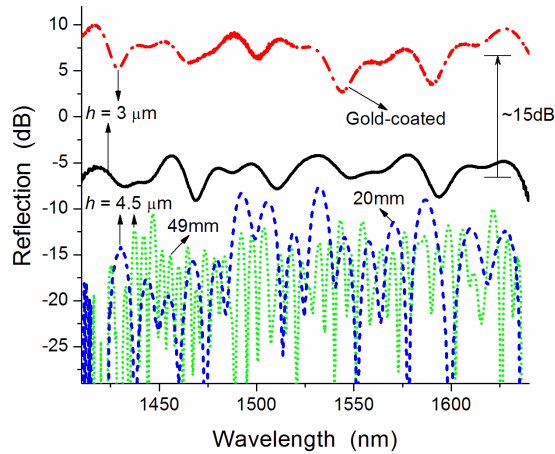


**Figure 3.** Relative reflection spectra of the four FMIs: gold-coated FMI with a lateral offset  $h = 3 \mu\text{m}$  (red dotted curve), uncoated FMI with a lateral offset  $h = 3 \mu\text{m}$  (black solid curve), uncoated FMI with a lateral offset  $h = 4.5 \mu\text{m}$  and a 49-mm sensing SMF (green dotted curve), and uncoated FMI with a lateral offset  $4.5 \mu\text{m}$  and a 20-mm sensing SMF (blue dashed curve).

SMF will change due to the stress-optic effect [18], which consequently results in the wavelength shift of the interference spectrum of the FMI. To show the performance of the proposed hydrostatic pressure sensor based on the FMI, we experimentally measure the reflection spectra of the proposed hydrostatic pressure sensor based on a gold-coated FMI based on a 12-mm sensing SMF with a lateral offset  $h = 3 \mu\text{m}$  under different hydrostatic pressures from 0 to 42 MPa with a step of 3 MPa, which are shown in the inset of Figure 4. Note that the wavelength range is limited to cover one period of the relative reflection spectra with one trough wavelength around 1545 nm for a high accurate measurement of the wavelength shift of the spectra. The wavelength shift of the relative reflection spectra is quite small. In order to achieve more accurate information which the relative reflection spectra of the hydrostatic pressure sensor carry, we use a polynomial expression by fitting a curve for the relative reflection spectra. For example, we achieve the trough wavelengths of the relative reflection spectra by calculating the axis of symmetry of a second-order polynomial which is achieved by fitting the relative reflection spectra curve in a wavelength range of 1 nm.

Figure 4 shows trough wavelengths (around 1545 nm) of the

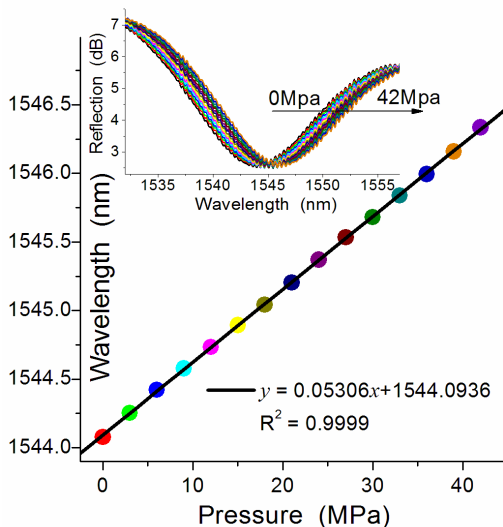


**Figure 4.** Trough wavelengths of the reflection spectra of the hydrostatic pressure sensor versus hydrostatic pressure. Inset shows the experimentally measured reflection spectra of the hydrostatic pressure sensor under different hydrostatic pressures from 0 to 42 MPa.

reflection spectra of the proposed hydrostatic pressure sensor versus hydrostatic pressure. A linear relationship between the hydrostatic pressure and wavelength shift of the trough wavelength of the relative reflection spectra is observed. The sensitivity of the pressure sensor is about 53 pm/MPa (or 0.019 MPa/pm), which is much larger than that of the previously reported FBG hydrostatic pressure sensor [18]. The maximum hydrostatic pressure applied to the sensor is 42 MPa, which is limited by the sealed oil tank and the high pressure hydraulic pump in our laboratory. The proposed hydrostatic pressure sensor is expected to have a much larger sensing range up to hundreds of MPa.

#### 4. DISCUSSIONS AND CONCLUSION

Although the recently developed photonic crystal fibers have been used to further improve the performance of the hydrostatic pressure sensor based on optical fibers, the SMF is still a good candidate due to the low cost and the ease to connect the optical source. The length of our previously reported FMI pressure sensor based on a few mode fiber is relative large since the FMI is based on two fiber core modes of

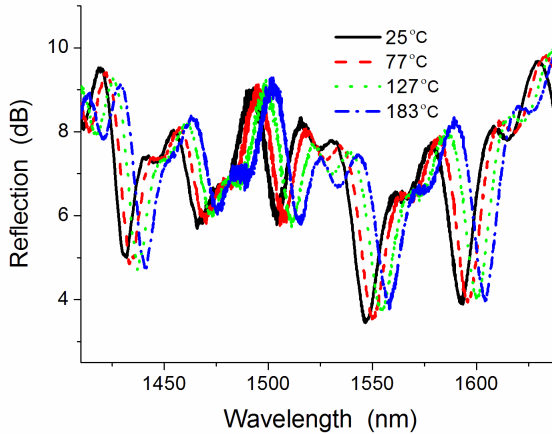


**Figure 5.** Measured relative reflection spectra of the gold-coated FMI under temperature of 25 °C, 77 °C, 127 °C, and 183 °C, respectively.

the few mode fiber and they have a very small difference of the mode indices which results in a large  $L$  for a suitable wavelength spacing according to Equation (2). The proposed FMI have a relatively short length due to the larger difference of the mode indices between the core mode and the cladding mode of the SMF. In practical applications of the pressure sensor, other environmental variables such as strain and temperature should also be considered. The pressure sensor should be well fixed in the sensing environment to avoid any strain which may be introduced by bending. For the temperature influence, we experimentally measured relative reflection spectra of the gold-coated FMI under temperature of 25 °C, 77 °C, 127 °C, and 183 °C, respectively, which are shown in Figure 5. The temperature change will also result in the wavelength shift with a sensitivity of about 75 pm/°C, which indicate a temperature sensor should also be used together with the pressure sensor. So far the temperature cross-talk has been one of the changing problems for most fiber-based pressure sensors. When the influence of the temperature and strain are ignored, the uncertainty of the pressure sensor is very low (less than 0.1%).

In conclusion, we have proposed and demonstrated a hydrostatic pressure sensor based on a gold-jacketed FMI formed by lateral splicing of the SMF. The pressure sensor can have a length even as short as several millimeters. An experimental setup of the proposed hydrostatic pressure sensor has been conducted and the results shown that applied hydrostatic pressure to the pressure sensor caused a red-shift of

the relative reflection spectrum of the pressure sensor. The linear relationship between the hydrostatic pressure and the wavelength shift of the relative reflection spectrum of the pressure sensor has been presented. The pressure sensor has been demonstrated with a sensitivity of 53 pm/MPa and a measurement range larger than 40 MPa.

## ACKNOWLEDGMENT

This work was supported partially by the National Natural Science Foundation of China under project (No. 61007029), Projects of Zhejiang Province (No. 2011C21038 and No. 2010R50007), Program for Science and Technology Innovative Research Team in Zhejiang Normal University, and the Central Research Grant of The Hong Kong Polytechnic University under the Postdoctoral Fellowship (Project No. G-YX2D).

## REFERENCES

1. Niklès, M., L. Thévenaz, and P. A. Robert, "Simple distributed fiber sensor based on Brillouin gain spectrum analysis," *Opt. Lett.*, Vol. 21, 758–760, 1996.
2. Kersey, A. D., M. A. Davis, H. J. Patrick, M. LeBlanc, K. P. Koo, C. G. Ashins, M. A. Putnam, and E. J. Friebele, "Fiber grating sensors," *J. Lightw. Technol.*, Vol. 15, 1442–1463, 1997.
3. Hill, K. O. and G. Meltz, "Fiber Bragg grating technology fundamentals and overview," *J. Lightw. Technol.*, Vol. 5, 1263–1276, 1997.
4. Farahani, M. A. and T. Gogolla, "Spontaneous raman scattering in optical fibers with modulated probe light for distributed temperature raman remote sensing," *J. Lightw. Technol.*, Vol. 17, 1379–1391, 1999.
5. Guan, B.-O., H.-Y. Tam, X.-M. Tao, and X.-Y. Dong, "Simultaneous strain and temperature measurement using a superstructure fiber Bragg grating," *IEEE Photon. Technol. Lett.*, Vol. 12, 675–677, 2000.
6. Culshaw, B., "Optical fiber sensor technologies: Opportunities and - perhaps - pitfalls," *J. Lightw. Technol.*, Vol. 22, 39–50, 2004.
7. Chen, D., C. Shu, and S. He, "Multiple fiber Bragg grating interrogation based on a spectrum-limited Fourier domain mode locking fiber laser," *Opt. Lett.*, Vol. 33, 1395–1397, 2008.

8. Chen, D., W. Liu, M. Jiang, and S. He, "High resolution strain/temperature sensor system based on high finesse fiber Bragg grating Fabry-Perot cavity and wavelength demodulation in the time domain," *J. Lightw. Technol.*, Vol. 27, 2477–2481, 2009.
9. Liu, S. C., Z. W. Yin, L. Zhang, X. F. Chen, L. Gao, and J. C. Cheng, "Dual-wavelength FBG laser sensor based on photonic generation of radio frequency demodulation technique," *Journal of Electromagnetic Waves Applications*, Vol. 23, No. 16, 2177–2185, 2009.
10. Sun, N.-H., J.-J. Liao, Y.-W. Kiang, S.-C. Lin, R.-Y. Ro, J.-S. Chiang, and H.-W. Chang, "Numerical analysis of apodized fiber Bragg gratings using coupled mode theory," *Progress In Electromagnetics Research*, Vol. 99, 289–306, 2009.
11. Liao, J.-J., N.-H. Sun, S.-C. Lin, R.-Y. Ro, J.-S. Chiang, C.-L. Pan, and H.-W. Chang, "A new look at numerical analysis of uniform fiber Bragg gratings using coupled mode theory," *Progress In Electromagnetics Research*, Vol. 93, 385–401, 2009.
12. Wang, B., G. Somesfalean, L. Mei, H. Zhou, C. Yan, and S. He, "Detection of gas concentration by correlation spectroscopy using a multi-wavelength fiber laser," *Progress In Electromagnetics Research*, Vol. 114, 469–479, 2011.
13. Ni, J., X. M. Zhang, S. L. Zheng, X. F. Jin, H. Chi, and X. M. Zhang, "Microwave frequency measurement based on phase modulation to intensity modulation conversion using fiber Bragg grating," *Journal of Electromagnetic Waves Applications*, Vol. 25, No. 5, 755–764, 2011.
14. Bock, W. J. and A. W. Domanski, "Highly hydrostatic pressure effects in highly birefringent optical fibers," *J. Lightw. Technol.*, Vol. 7, 1279–1283, 1989.
15. Charasse, M. N., M. Turpin, and J. P. Le Pesant, "Dynamic pressure sensing with a side-hole birefringent optical fiber," *Opt. Lett.*, Vol. 16, 1043–1045, 1991.
16. Clowes, J. R., S. Syngellakis, and M. N. Zervas, "Pressure sensitivity of side-hole optical fiber sensors," *IEEE Photon. Technol. Lett.*, Vol. 10, 857–859, 1998.
17. Fu, H. Y., H. Y. Tam, L. Y. Shao, X. Dong, P. K. A. Wai, C. Lu, and S. K. Khijwania, "Pressure sensor realized with polarization-maintaining photonic crystal fiber-based Sagnac interferometer," *Appl. Opt.*, Vol. 47, 2835–2839, 2008.
18. Wu, C., B. O. Guan, Z. Wang, and X. Feng, "Characterization of pressure response of Bragg gratings in grapefruit microstructured

- fibers,” *J. Lightw. Technol.*, Vol. 28, 1392–1397, 2010.
19. Szczurowski, M. K., T. Martynkien, G. Statkiewicz-Barabach, W. Urbanczyk, and D. J. Webb, “Measurements of polarimetric sensitivity to hydrostatic pressure, strain and temperature in birefringent dual-core microstructured polymer fiber,” *Opt. Express*, Vol. 18, 12076–12087, 2010.
  20. Fu, H. Y., C. Wu, M. L. V. Tse, L. Zhang, K. C. D. Cheng, H. Y. Tam, B. O. Guan, and C. Lu, “High pressure sensor based on photonic crystal fiber for downhole application,” *Appl. Opt.*, Vol. 49, 2639–2644, 2010.
  21. Martynkien, T., G. Barabach, J. Olszewski, J. Wojcik, P. Mergo, T. Geernaert, C. Sonnenfeld, A. Anuszkiewicz, M. K. Szczurowski, K. Tarnowski, M. Makara, K. Skorupski, J. Klimek, K. Poturaj, W. Urbanczyk, T. Nasilowski, F. Berghmans, and H. Thienpont, “Highly birefringent microstructured fibers with enhanced sensitivity to hydrostatic pressure,” *Opt. Express*, Vol. 18, 15113–15121, 2010.
  22. Chen, D., G. Hu, and L. Chen, “Dual-core photonic crystal fiber for hydrostatic pressure sensing,” *IEEE Photon. Technol. Lett.*, Vol. 23, 1851–1853, 2011.
  23. Chen, D., G. Hu, M.-L. V. Tse, and H. Y. Tam, “Dual-core side-hole fiber for pressure sensing based on intensity detection,” *Journal of Electromagnetic Waves Applications*, Vol. 25, Nos. 5–6, 775–784, 2011.
  24. Chen, D., M. L. V. Tse, C. Wu, G. Hu, H. Y. Tam, and L. Gao, “Highly birefringent four-hole fiber for pressure sensing,” *Progress In Electromagnetics Research*, Vol. 114, 145–158, 2011.
  25. Zhu, Y. and A. Wang, “Miniature fiber-optic pressure sensor,” *IEEE Photon. Technol. Lett.*, Vol. 17, 447–449, 2005.
  26. Wang, X., J. Xu, Y. Zhu, K. L. Cooper, and A. Wang, “All-fused-silica miniature optical fiber tip pressure sensor,” *Opt. Lett.*, Vol. 31, 885–887, 2006.
  27. Wang, W., N. Wu, Y. Tian, C. Niezrecki, and X. Wang, “Highly birefringent microstructured fibers with enhanced sensitivity to hydrostatic pressure,” *Opt. Express*, Vol. 18, 9006–9014, 2010.
  28. Knight, J. C., J. Broeng, T. A. Birks, and P. S. J. Russell, “Photonic band gap guidance in optical fibers,” *Science*, Vol. 282, 1476–1478, 1998.
  29. Knight, J. C. and P. S. J. Russell, “Photonic crystal fibers: New way to guide light,” *Science*, Vol. 296, 276–277, 2002.
  30. Knight, J. C., “Photonic crystal fibers,” *Nature*, Vol. 424, 847–

- 851, 2003.
31. Nozhat, N. and N. Granpayeh, "Specialty fibers designed by photonic crystals," *Progress In Electromagnetics Research*, Vol. 99, 225–244, 2009.
  32. Choudhury, P. K. and W. K. Soon, "TE mode propagation through tapered core liquid crystal optical fibers," *Progress In Electromagnetics Research*, Vol. 104, 449–463, 2010.
  33. Ortigosa-Blanch, A., J. C. Knight, W. J. Wadsworth, J. Arriaga, B. J. Mangan, T. A. Birks, and P. S. J. Russel, "Highly birefringent photonic crystal fibers," *Opt. Lett.*, Vol. 25, 1325–1327, 2000.
  34. Hansen, T. P., J. Broeng, S. E. B. Libori, E. Knudsen, A. Bjarklev, J. R. Jensen, and H. Simonsen, "Highly birefringent index-guiding photonic crystal fibers," *IEEE Photon. Technol. Lett.*, Vol. 13, 588–590, 2001.
  35. Steel, M. J. and R. M. Osgood, "Elliptical-hole photonic crystal fibers," *Opt. Lett.*, Vol. 26, 229–231, 2001.
  36. Steel, M. J. and R. M. Osgood, "Polarization and dispersive properties of elliptical-hole photonics crystal fibers," *J. Lightw. Technol.*, Vol. 19, 495–503, 2001.
  37. Sapulak, M., G. Statkiewicz, J. Olszewski, T. Martynkien, W. Urbanczyk, J. Wojcik, M. Makara, J. Klimek, T. Nasilowski, F. Berghmans, and H. Thienpont, "Experimental and theoretical investigations of birefringent holey fibers with a triple defect," *Appl. Opt.*, Vol. 44, 2652–2658, 2005.
  38. Chen, D. and L. Shen, "Highly birefringent elliptical-hole photonic crystal fibers with double defect," *J. Lightw. Technol.*, Vol. 25, 2700–2705, 2007.
  39. Yue, Y., G. Kai, Z. Wang, T. Sun, L. Jin, Y. Lu, C. Zhang, J. Liu, Y. Li, Y. Liu, S. Yuan, and X. Dong, "Highly birefringent elliptical-hole photonic crystal fiber with squeezed hexagonal lattice," *Opt. Lett.*, Vol. 32, 469–471, 2007.
  40. Chen, D. and L. Shen, "Ultrahigh birefringent photonic crystal fiber with ultralow confinement loss," *IEEE Photon. Technol. Lett.*, Vol. 19, 185–187, 2007.
  41. Ferrando, A., E. Silvestre, J. J. Miret, and P. Andres, "Nearly zero ultraflattened dispersion in photonic crystal fibers," *Opt. Lett.*, Vol. 25, 790–792, 2000.
  42. Ferrando, A., E. Silvestre, P. Andres, J. Miret, and M. Andres, "Designing the properties of dispersion-flattened photonic crystal fibers," *Opt. Express*, Vol. 9, 687–697, 2001.

43. Saitoh, K., M. Koshiba, T. Hasegawa, and E. Sasaoka, "Chromatic dispersion control in photonic crystal fibers: Application to ultra-flattened dispersion," *Opt. Express*, Vol. 11, 843–852, 2003.
44. Shen, L. P., W. P. Huang, and S. S. Jian, "Design of photonic crystal fibers for dispersion-related applications," *J. Lightw. Technol.*, Vol. 21, 1644–1651, 2003.
45. Gérôme, F., J.-L. Auguste, and J.-M. Blondy, "Design of dispersion-compensating fibers based on a dual-concentric-core photonic crystal fiber," *Opt. Lett.*, Vol. 29, 2725–2727, 2004.
46. Poletti, F., V. Finazzi, T. M. Monro, N. G. R. Broderick, V. Tse, and D. J. Richardson, "Inverse design and fabrication tolerances of ultra-flattened dispersion holey fibers," *Opt. Express*, Vol. 13, 3728–3736, 2005.
47. Huttunen, A. and P. Törmä, "Optimization of dual-core and microstructure fiber geometries for dispersion compensation and large mode area," *Opt. Express*, Vol. 13, 627–635, 2005.
48. Varshney, S. K., T. Fujisawa, K. Saitoh, and M. Koshiba, "Design and analysis of a broadband dispersion compensating photonic crystal fiber Raman amplifier operating in S-band," *Opt. Express*, Vol. 14, 3528–3540, 2006.
49. Yang, S., Y. Zhang, X. Peng, Y. Lu, S. Xie, J. Li, W. Chen, Z. Jiang, J. Peng, and H. Li, "Theoretical study and experimental fabrication of high negative dispersion photonic crystal fiber with large area mode field," *Opt. Express*, Vol. 14, 3015–3023, 2006.
50. Agrawal, A., N. Kejalakshmy, J. Chen, B. M. A. Rahman, and K. T. V. Grattan, "Golden spiral photonic crystal fiber: Polarization and dispersion properties," *Opt. Lett.*, Vol. 33, 2716–2718, 2008.
51. Chen, D., M.-L. V. Tse, and H. Y. Tam, "Optical properties of photonic crystal fibers with a fiber core of arrays of subwavelength circular air holes: Birefringence and dispersion," *Progress In Electromagnetics Research*, Vol. 105, 193–212, 2010.
52. Ju, J., W. Jin, and M. S. Demokan, "Design of single-polarization single mode photonics crystal fibers," *J. Lightw. Technol.*, Vol. 24, 825–830, 2001.
53. Saitoh, K. and M. Koshiba, "Single-polarization single-mode photonic crystal fibers," *IEEE Photon. Technol. Lett.*, Vol. 15, 1384–1340, 2003.
54. Kubota, H., S. Kawanishi, S. Koyanagi, M. Tanaka, and S. Yamaguchi, "Absolutely single polarization photonic crystal fiber," *IEEE Photon. Technol. Lett.*, Vol. 16, 182–184, 2004.

55. Knight, J. C. and D. V. Skryabin, "Nonlinear waveguide optics and photonic crystal fibers," *Opt. Express*, Vol. 15, 15365–15376, 2007.
56. Mortensen, N. A., M. D. Nielsen, J. R. Folkenberg, A. Petersson, and H. R. Simonsen, "Improved large-mode-area endlessly single-mode photonic crystal fibers," *Opt. Lett.*, Vol. 28, 393–395, 2003.
57. Limpert, J., T. Schreiber, S. Nolte, H. Zellmer, T. Tunnermann, R. Iliew, F. Lederer, J. Broeng, G. Vienne, A. Petersson, and C. Jakobsen, "High-power air-clad large-mode-area photonic crystal fiber laser," *Opt. Express*, Vol. 11, 818–823, 2003.
58. Folkenberg, J., M. Nielsen, N. Mortensen, C. Jakobsen, and H. Simonsen, "Polarization maintaining large mode area photonic crystal fiber," *Opt. Express*, Vol. 12, 956–960, 2004.
59. Wadsworth, W. J., J. C. Knight, W. H. Reewes, P. S. J. Russell, and J. Arriaga, "Yb<sup>3+</sup>-doped photonic crystal fibre laser," *Electron. Lett.*, Vol. 36, 1452–1253, 2000.
60. Liu, X., X. Zhou, X. Tang, J. Ng, J. Hao, T. Chai, E. Leong, and C. Lu, "Swiathable and tunable multiwavelength erbium-doped fiber laser with fiber Bragg grating and photonic crystal fiber," *IEEE Photon. Technol. Lett.*, Vol. 17, 1626–1628, 2005.
61. Chen, D., "Stable multi-wavelength erbium-doped fiber laser based on photonic crystal fiber Sagnac loop filter," *Laser Phys. Lett.*, Vol. 4, 437–439, 2007.
62. Broderick, N. G. R., T. M. Monro, P. J. Bennett, and D. J. Richardson, "Nonlinearity in holey optical fibers: Measurement and future opportunities," *Opt. Lett.*, Vol. 24, 1395–1397, 1999.
63. Zhu, Z. and T. G. Brown, "Experimental studies of polarization properties of supercontinua generated in a birefringent photonic crystal fiber," *Opt. Express*, Vol. 12, 791–796, 2004.
64. Zhu, Z. and T. G. Brown, "Polarization properties of supercontinuum spectra generated in birefringent photonic crystal fibers," *J. Opt. Soc. Am. B*, Vol. 21, 249–257, 2004.
65. Dudley, J. M. and J. R. Taylor, "Ten years of nonlinear optics in photonic crystal fibre," *Nature Photonics*, Vol. 3, 85–90, 2009.
66. Dong, X. and H. Y. Tam, "Temperature-insensitive strain sensor with polarization-maintaining photonic crystal fiber based on Sagnac interferometer," *Appl. Phys. Lett.*, Vol. 90, 151113–151115, 2007.
67. Ritari, T., J. Tuominen, H. Ludvigsen, J. C. Petersen, T. Sørensen, T. P. Hansen, and H. R. Simonsen, "Gas sensing

- using air-guiding photonic crystal bandgap fibers,” *Opt. Express*, Vol. 12, 4080–4087, 2004.
68. Rindorf, L., J. B. Jensen, M. Dufva, L. H. Pedersen, P. T. Høiby, and O. Bang, “Photonic crystal fiber long-period gratings for biochemical sensing,” *Opt. Express*, Vol. 14, 8224–8231, 2006.
  69. Wu, D. K. C., B. T. Kuhlmeier, and B. J. Eggleton, “Ultrasensitive photonic crystal fiber refractive index sensor,” *Opt. Lett.*, Vol. 34, 322–324, 2009.
  70. Qian, W. W., C.-L. Zhao, S. L. He, X. Y. Dong, S. Q. Zhang, Z. X. Zhang, S. Z. Jin, J. T. Guo, and H. F. Wei, “High-sensitivity temperature sensor based on an alcohol-filled photonic crystal fiber loop mirror,” *Opt. Lett.*, Vol. 36, 1548–1550, 2011.
  71. Chen, D., C. Wu, M.-L. V. Tse, and H. Y. Tam, “Hydrostatic pressure sensor based on mode interference of a few mode fiber,” *Progress In Electromagnetics Research*, Vol. 119, 335–343, 2011.